THE JOURNAL OF PHYSICAL CHEMISTRY B

ARTICLE

pubs.acs.org/JPCB

Low-Temperature Frequency Domain Study of Excitation Energy Transfer in Ethynyl-Linked Chlorophyll Trefoils and Aggregates

Bhanu Neupane,[†] Nhan C. Dang,[†,§] Richard F. Kelley,[‡] Michael R. Wasielewski,[‡] and Ryszard Jankowiak*[,†]

[†]Department of Chemistry, Kansas State University, Manhattan, Kansas 66506, United States

[‡]Department of Chemistry and Argonne-Northwestern Solar Energy Research (ANSER) Center, Northwestern University, Evanston, Illinois 60208, United States

ABSTRACT: Using hole-burning spectroscopy, we show that excitation energy transfer (EET) time in ethynyl-linked chlorophyll trefoil (ChlT1) monomer is very fast (~2.5 ps) at liquid helium temperature. This is consistent with data obtained by femtosecond transient spectroscopy experiments performed at room temperature, in which an EET time of 1.8 ps was observed (Kelley, R. F. et al. *Angew. Chem. Int. Ed.* **2006**, *45*, 7979). This finding further supports the importance of through-bond electronic coupling at low temperature. In addition, we show that ChlT1 (even at very low concentrations) in methyl tetrahydrofuran−ethanol glass (1:200 v/v; $T \sim 5$ K) forms different types of aggregates. It is demonstrated that the relative distribution of various types of aggregates (whose possible structures are briefly discussed) depends on the cooling rate and matrix composition. For example, the EET time in two types of ChlT1-based aggregates is slower by a factor of ~5−7 with respect to that observed for ChlT1 monomer. This indicates that ChlT1 aggregates can retain ultrafast energy transfer properties similar to those observed in natural photosynthetic antennas. It is anticipated that such building blocks could be utilized in future photovoltaic devices.

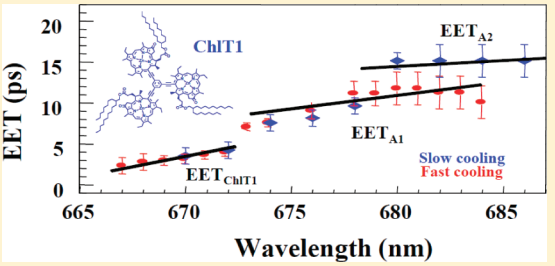

1. INTRODUCTION

Natural photosystems contain chlorophylls (Chls) as major building blocks to harvest solar energy in the formation of a charge-separated state. Different protein subunits optimize the overall process of photosynthesis in space, frequency, and time, resulting in a photon-to-charge conversion efficiency close to 100%.[1−4] Inspired by natural photosynthesis, different groups[5−22] are interested in mimicking natural photosynthesis using different types of synthetic molecules, including chlorophyll trefoils (ChlTs). These molecules consist of three identical zinc−Chl subunits connected by rigid linkers (ethynyl or phenyl−ethynyl) to the central benzene unit, facilitating EET through both space and bond energy transfer.[23] The beauty of these molecules is that, depending on solvent polarity, temperature, and their concentration, they self-aggregate to form building blocks of different sizes, thus increasing absorption efficiency and also making multidirectional energy flow possible. In this regard, ChlTs seem to be well optimized for very efficient light harvesting,[23] mimicking various natural photosynthetic antenna systems.[24−38]

Excitation energy transfer (EET) in ChlTs in THF was previously studied by room temperature transient absorption spectroscopy.[23] It was shown that EET in ChlT having ethynyl linkers (referred to below as ChlT1) is ~2 ps, about three times faster than in ChlT having phenyl−ethynyl linkers (labeled below as ChlT2).[23] This difference in EET between ChlT1 and ChlT2 is due to more effective through-space and through-bond coupling between zinc−Chl subunits in ChlT1.[23] Very recently, photophysical properties of ChlT1 and ChlT2 (along with their respective monomeric units M1 and M2) were studied at the single molecule level.[39] The later work demonstrated that ChlT1 is more photostable and less structurally flexible than ChlT2. This observed difference in properties between ChlT1 and ChlT2 was interpreted as a direct result of stronger electronic coupling and more rigid linkers in ChlT1.[23,39]

In this manuscript, we further characterize ChlT1 and its aggregates using spectral hole-burning (HB) spectroscopy. This is a well-known and powerful frequency domain technique to study EET and excitonic structure in complex biomolecules.[40−44] The low-temperature aggregates ($T = 5$ K) are formed in 2-methyltetrahydofuran (MTHF) and ethanol glass (~1:200 v/v); changing the stoichiometric ratio of ethanol, MTHF, and water controls the composition of the room temperature aggregates. Findings of the HB experiments are compared with femtosecond pump−probe experiments[23] and the recently obtained single trefoil data.[39] We anticipate that further characterization of ChlT1 and its aggregates will provide more information on the structure−function relationship in these interesting systems and will pave the way for design of better artificial antennae for light-harvesting in future photovoltaic devices. Possible structures of ChlT1 aggregates are discussed in light of previously published data obtained for Chl *a* aggregates.[45−54] In particular, we point out that not only ChlT1 monomer, but also various self-aggregated

Received: March 23, 2011
Revised: August 5, 2011
Published: August 05, 2011

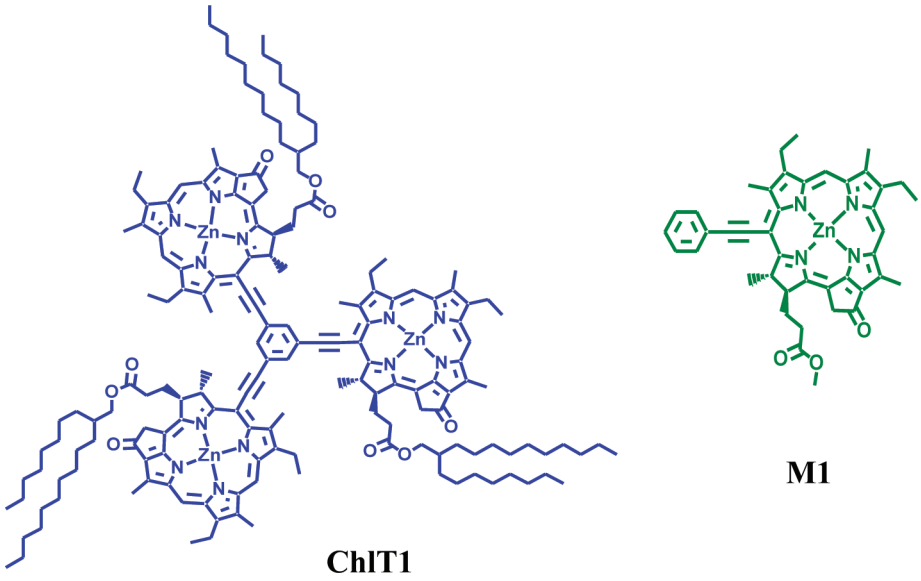

Figure 1. Structure of trefoil (ChlT1) and its monomer (M1).

trefoils, carry out ultrafast excitation energy transfer. It is shown that EET time is slower in large aggregates by a factor of about 5−7 with respect to that observed for ChlT1 (2.5 ps).

2. MATERIALS AND METHODS

2.1. Sample Preparation. The approach for synthesis of chlorophyll trefoil (ChlT1) and its monomeric subunit (M1) is described in ref 23. Sample preparation for spectroscopic measurements was performed in a nitrogen-purged atmosphere using 2-methyltetrahydrofuran (Acros Organics, extra dried over molecular sieve, 99+% purity and molecular weight of 86.13) and ethanol (Pharmaco-Aaper, absolute ACS/USP grade, 99.98% purity with 0.02% water) as solvents. Solvent stoichiometry and concentrations of ChlT1 and M1 used are given in the figure captions. Cooling time required for reaching 5 K, for slow- and fast-cooling samples, was ∼20 and ∼2 min, respectively.

2.2. Spectroscopic Measurement. A detailed description of our HB setup can be found in refs 35 and 36. Briefly, low-temperature absorption and HB spectra were recorded with a Bruker HR125 Fourier transform spectrometer at a resolution of either 4 or 0.5 cm^{-1}. Nonresonant HB was performed with the green 496.5 nm line from a Coherent Innova 200 Ar^+ ion laser. A tunable Coherent CR699-21 ring-dye laser (line width of 0.07 cm^{-1}, laser dye: DCM Special (Exciton)), pumped by a 6-W Coherent Innova 90 Ar^+ ion laser, was used for resonant HB. The intensity of the CR699-21 laser beam was stabilized electro-optically (Brockton Electro-Optics Corp., LPC) and was attenuated (if needed) using a set of neutral-density filters. The persistent nonphotochemical HB spectra reported correspond to the postburn absorption spectrum minus the preburn absorption spectrum. Burn wavelengths, intensities, and times are given in the figure captions. Fluorescence spectra were obtained with an excitation wavelength of 496.5 nm from the Coherent Innova 200 Ar^+ ion laser. Fluorescence was dispersed by a 300-mm focal-length monochromator and detected by a PI Acton Spec-10 (1340 × 400) back-illuminated CCD camera. Spectral resolution for the fluorescence spectra was ∼0.1 nm. The sample temperature was maintained at 5 K (unless otherwise specified) using a Janis 8-DT Super Vari-Temp liquid helium cryostat. The

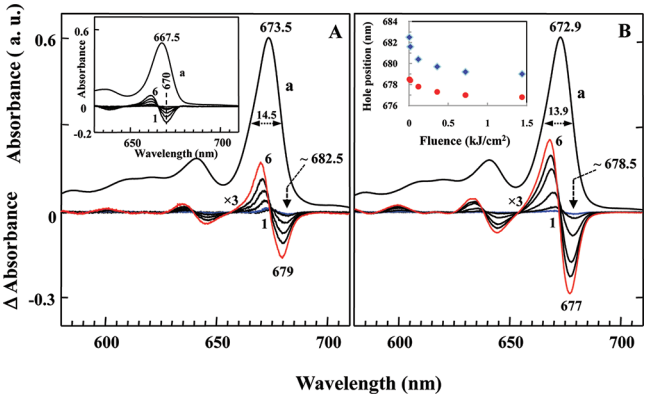

Figure 2. Frame A: Curve a shows the absorption spectrum of sample 1s at 5 K. Spectra labeled 1−6 are nonresonant holes obtained at various stages of hole burning (from low to high fluence) at a burning frequency of 496.5 nm. Inset in frame A shows absorption (curve a) and HB spectra (labeled 1−6) for M1 obtained under conditions identical to that for sample 1s. Frame B: Absorption spectrum (curve b) and nonresonant holes (labeled 1−6) for fast-cooled sample (2f). For clarity, spectra labeled 1−6 in both frames are magnified by a factor of 3. Centroid of the Q_y hole minimum as a function of fluence for sample 1s (blue diamonds) and 2f (red circles) is plotted in the inset of frame B. Trefoil concentration, $c \sim 2 \times 10^{-5}$ M; stoichiometric ratio of solvent (MTHF/C_2H_5OH ∼ 1:200 v/v).

temperature was stabilized and measured with a Lakeshore Cryotronic model 330 temperature controller. For resonant Raman spectra, a He−Ne laser (λ = 630 nm, $I \sim 10$ mW/cm^2) was focused on a glass slide with a concave well that could hold ∼60 μL of solution, and spectra were measured using a confocal Raman microspectroscope (Horiba Jobin-Yvon microscope and iHR 550 spectrometer) at a resolution of ∼2 cm^{-1}. During measurement, the sample was covered with a microscope slide to prevent possible solvent evaporation and signal fluctuation.

3. RESULTS

3.1. Absorption, Nonresonant HB, and Fluorescence Spectra for Fast- and Slow-Cooled Samples of ChlT1 at 5 K. Figure 1

Table 1. Spectral Characteristics and Relative Contribution of Trefoils (ChlT1) and A1−A4 Aggregates in Slowly (1s) and Fast-Cooled (2f) Samples at 5 K

pigment nomenclature and spectral maxima			relative contribution	
name	absorption (nm)	fluorescence (nm)	fast cooling	slow cooling
ChlT1	∼676.5 ± 1	678 ± 1	major	minor
A1	*a*	*a*	minor	moderate
A2	∼682.5 ± 1	∼685 ± 1	very minor	major
A3	∼703 ± 2[b]	∼720 ± 2	minor	minor
A4	*c*		*c*	*c*

[a] The maximum of the A1-type aggregates appears to be near 677 nm, although its exact position cannot be provided. Nevertheless, data shown in Figures 2 and 6 indicate that A1 is present in both samples 1s and 2f but at different concentrations. Trefoil-based A1 aggregates appear to be only slightly red-shifted in comparison with ChlT1, but they have a lower energy (0, 0) band than the A2 aggregates; see text for details. [b] The lowest excitonic state is near 710 nm, although the absorption peak appears to be ∼703 ± 2 nm; see Figure 3B. [c] The positive increase in absorption beyond 730 nm is an indication that such aggregates exist in minor amounts in both slow- and fast-cooling samples at 5 K; see Figure 3B. Absorption beyond 740 nm was not measured for these samples. Nevertheless, such aggregates are clearly revealed at room temperature in water-based solvents (see Figure 5A).

shows the chemical structure of ChlT1 and its individual monomer (referred to as M1) studied in this work. The 5 K absorption spectra obtained for sample 1s (s stands for slow cooling; curve a) and sample 2f (f indicates fast cooling; curve a) are shown in Figure 2 in frames A and B, respectively. Note that absorption spectrum of the slowly cooled sample is slightly broader and red-shifted with more absorption, particularly in the spectral range of 680−710 nm. HB spectra in both frames (labeled 1−6) were obtained using the same fluence of 6, 18, 120, 360, 540, and 1440 J/cm^2. Spectra labeled 1 and 6 in both frames represent HB spectra obtained in the very early stages of the HB process (i.e., so-called shallow holes) and saturated holes. The depth of the saturated holes in frames A and B is 21% and 19%, respectively. Note that the shape and spectral position of curves 1−6 depend on the cooling rate. The centroid of the Q_y hole minimum for sample 1s (blue data points) and sample 2f (red data points) is plotted as a function of fluence in the inset of frame B. It is apparent that hole position in a slowly cooled sample (1s) shifts faster (by a factor of 2) toward higher energies when compared with the fast-cooled sample (2f). This different behavior is caused by a different degree of aggregation because these molecules were designed to self-assemble.[23]

Data presented in Figure 2 clearly show that sample 2f, with its blue-shifted absorption origin band and nonresonant HB spectra, has more contribution from ChlT1 monomers (i.e., it represents a less aggregated sample) than sample 1s. Note the difference in full-width-at-half-maximum (fwhm) and HB characteristics. Spectral differences observed in frames A and B of Figure 2 are not surprising because a similar effect of cooling rate on absorption and emission spectra was previously observed for Chl *a* molecules.[44,50] For clarity of discussion, the following nomenclature is adopted below: monomer trefoils are labeled ChlT1 (as above), and different types of aggregates will be referred to as A*i* (*i* = 1, 2, 3, 4) aggregates. For example, the aggregates with the most blue- and red-shifted origin bands are labeled as A1 and A4, respectively. We will argue below that both samples 1s and 2f consist of four types of aggregates (i.e. A1−A4), but their relative contribution is very different. A summary of the various aggregates formed in both types of samples as well as the corresponding spectral band positions and relative contributions are presented in Table 1 (see also section 4.1 for discussion). The possible nature of all aggregates is discussed in section 4.2. For completeness, we add that absorption and HB spectra for monomer sample M1 (see inset of Figure 2A) were also measured at conditions identical to those for sample 1s. Since M1 consists of only one chlorophyll unit, its Q_y (0, 0) origin band is significantly blue-shifted, with an absorption maximum near 667.5 nm. In this case, as expected for isolated (noninteracting) pigments in a glassy matrix, the nonresonant hole does not shift with fluence. Below, we focus on ChlT1 and its possible aggregates that could be used as artificial antenna systems in future photovoltaic devices.

The major contribution in sample 1s originates from A2 aggregate, and contributions from A1, A3, A4 in sample 2f are minor; therefore, the difference of two normalized saturated HB spectra obtained for samples 1s and 2f can reveal a contribution from ChlT1 in sample 2f. Such normalized saturated persistent HB spectra for samples 1s (curve a) and 2f (curve b) are replotted in Figure 3A. Curve c in frame A represents the difference between curves b and a and is assigned to the low-energy state of ChlT1 monomer (∼676.5 nm). Saturated HB spectra (curves a and b from frame A) and the corresponding absorption spectra (curves c and d, respectively) are shown with a longer wavelength range in frame B for comparison. The spectral feature peaking near 703 nm is an indication of a new type of aggregate, referred to below to as an A3 aggregate. To guide the eyes, the broad hole (fwhm ∼ 500 cm^{-1}) observed in curve a is fitted with an inverted Gaussian (curve e), peaking at ∼710 nm and suggesting this is the position of the lowest energy state in the type A3 aggregate. Interestingly, the absorbance does not go to zero beyond 730 nm, indicating the presence of another form of aggregate, labeled below as A4 (see also Figure 5A). Proof that aggregates A1 and A2 also exist at low temperatures (even at relatively low ChlT1 concentrations) is provided in section 3.2.

At this point, we turn to normalized fluorescence spectra obtained for samples 1s and 2f that are presented in Figure 4 as curves a and b. Note that the (0, 0) band in spectrum a is red-shifted by 6.5 nm in comparison with spectrum b; in addition, spectrum a shows an additional emission band near 720 nm, as indicated by an asterisk. As expected, the emission maximum is red-shifted upon aggregation. The presence of similar emission bands was previously observed for special Chl *a* dimers (i.e., $(Chla \cdot H_2O)_2$) in different solvents, as demonstrated in refs 45, 53, 54. In the case of our trefoil samples, the ∼720 nm emission band is assigned to type A3 aggregates; see section 4.2 for discussion. On the basis of the emission maximum in curve b (i.e., 678.5 nm) and the position of the shallow nonresonant hole at the same wavelength (678.5 nm; curve 1 in frame B of Figure 2), we conclude that the fluorescence band with the (0, 0) band at 678.5 nm (curve b) is contributed to by trefoils (ChlT1; major contribution) and type A1 aggregates (minor contribution). Hole position and relative blue shift as a function of fluence strongly depend on the degree of aggregation. The emission maximum near 685 nm is assigned to type A2 aggregates, but a small contribution from ChlT1 monomer and A1 aggregates cannot be excluded, as shown by spectrum c, which

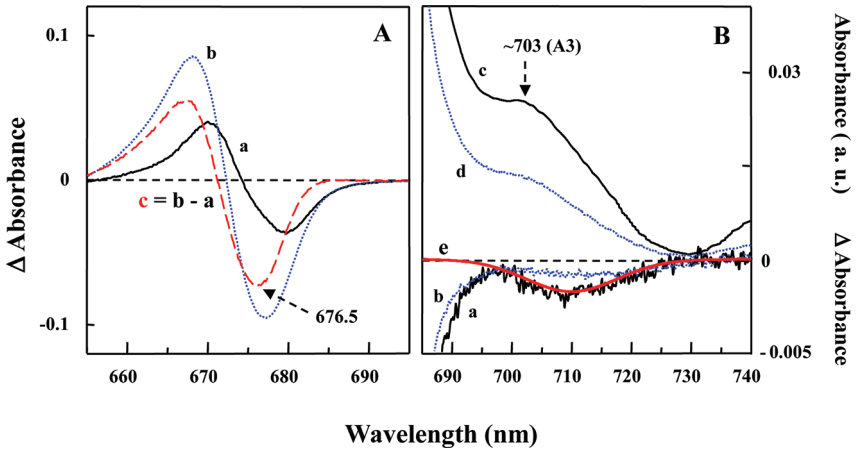

Figure 3. Frame A: Saturated nonresonant HB spectra for samples 1s (spectrum a) and 2f (spectrum b) normalized at 685.0 nm. The difference between spectra a and b is shown as curve c. Frame B: Curves a and b are the saturated nonresonant holes obtained for samples 1s and 2f, respectively, in the longer wavelength range. Corresponding absorption spectra are shown for comparison. Simple Gaussian fit to the broad hole in curve a is shown as curve e.

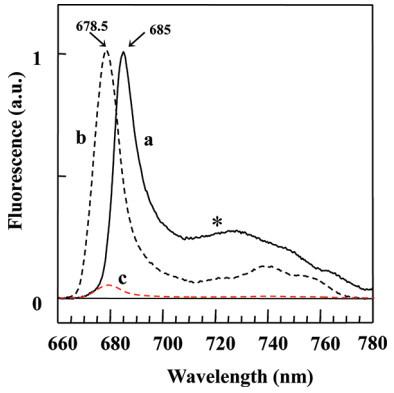

Figure 4. Curves a and b are normalized 5 K fluorescence spectra obtained for samples 1s and 2f, respectively. Both spectra were obtained at the same excitation wavelength of 496.5 nm with a laser power density of 0.5 mW/cm^2.

corresponds to spectrum b scaled by a factor of 0.08. (Note that HB and fluorescence quantum yields in the case of aggregates may not be same, so their relative contributions may differ).

3.2. Room Temperature Study. To confirm whether the above-mentioned aggregates (i.e. A1−A4) observed in low-temperature spectra are formed at room temperature, we measured the absorption spectra of ChlT1 samples at 298 K with a varying stoichiometric ratio of water. Results are presented in Figure 5A. The observed change in spectral position, bandwidth, and relative absorption intensity with an increased concentration of water (see curves a−d; with d having the largest concentration of water) is apparent. The continuous increase in absorbance in the longer wavelength region clearly indicates formation of various aggregates. Similar behavior was previously observed for aggregated Chl *a* molecules.[46] It appears that all four types of aggregates mentioned above are present. It is interesting to note that A4 (~740 nm) and A3 (~700 nm) types of aggregates are preferentially formed with an increase in water concentration. Figure 5B shows the resonance Raman spectrum obtained for trefoils embedded into the MTHF/ethanol/water mixture (1:45:45 v/v) to provide more insight into the aggregation process; see section 4.2 for discussion.

3.3. ZPH Action Spectra. ZPH action spectroscopy[42,43] allows investigation of the position of the lowest energy state of various molecular systems embedded in a glassy matrix at low temperatures. In this approach (absorption mode), the burn wavelength (λ_B) dependence of shallow (~10%) ZPH depth is measured under constant fluence.[42,43] Inverted ZPH holes obtained for samples 1s (blue) and 2f (red) at 5 K are shown in Figure 6A. Holes were burnt using a fluence of ~1 J/cm^2 at a resolution of 0.5 cm^{-1}. As expected, a comparison of the ZPH action spectra for the slow- and fast-cooled systems differ with deeper, narrower, and red-shifted holes observed for the slowly cooled sample (1s). The latter indicates different compositions of the low-energy state with significantly lower contribution from trefoils. Estimated EET times using eq 1[40,41] (from the hole-widths corrected for resolution) are plotted as a function of λ_B in frame B of Figure 6.

$$\Gamma_{hom} = (1/2\pi cT_1 + 1/2\pi c\tau_{EET}) + 1/\pi cT_2^* \approx 1/2\pi c\tau_{EET} \quad (1)$$

In eq 1, Γ_{hom} is the homogeneous line width (half-width-at-half-maximum of ZPH), T_1 is the fluorescence lifetime, T_2^* is the "pure" dephasing time, and τ_{EET} is the excitation energy transfer time.[40,41,43] For example, the ZPH width of 4.5 cm^{-1}, after correction for our resolution, corresponds to an EET time of ~2.5 ps. Frame B of Figure 6 shows measured EET times for a slowly cooled sample (blue data points) and a fast-cooled sample (red data points). The slanted solid lines in frame B are to assist graph interpretation. Contributions from A3 and A4 aggregates in the matrix (MTHF/C_2H_5OH ~ 1:200 v/v) were too low to measure corresponding ZPH action spectra. Nevertheless, three distinct EET time regions within the 667−686 nm region indicate that EET dynamics depend on extent and type of aggregation (vide infra).

4. DISCUSSION

4.1. Low-Temperature Absorption, HB, and Fluorescence Spectra. It is well-known that Chls and Chl-like molecules are highly susceptible to aggregation. The level of aggregation depends primarily on concentration, temperature, and matrix

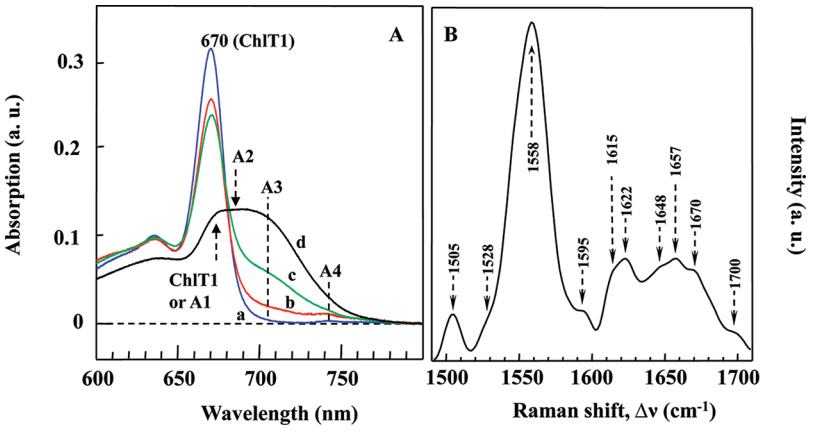

Figure 5. Frame A: Spectral changes observed in the absorption spectrum of trefoils with an increasing amount of water at $T = 298$ K. In spectra a−d, the solvent stoichiometry reported as H_2O/C_2H_5OH/MTHF (v/v) was 0:16:1, 2:14:1, 3:13:1, and 8:8:1, respectively. The trefoil concentration was ∼1.5 × 10^{-5} M. Frame B: Resonant Raman spectrum of a trefoil sample (∼10^{-4} M) prepared in a H_2O/C_2H_5OH/MTHF (45:45:1 v/v) mixture.

composition.[44,45,50−53] However, the cooling rate was also reported to affect the degree of aggregation and the shape of the optical spectra for Chl a, as reported in refs 44 and 50. Typically, red-shifted and broader absorption origin bands for Chl-like molecules indicate aggregation.[44−54] This is clearly observed when the absorption spectrum in frame A of Figure 2 for sample 1s is compared with the absorption spectrum shown in frame B for sample 2f. The difference in sample composition is more pronounced when the nonresonant holes (curves 1−6) shown in frames A and B of Figure 2 are compared. Note the different hole positions for shallow and saturated holes. In addition, the blue shift of saturated holes in fast-cooled samples (2f) is a factor of ∼2.3 smaller than that in sample 1s (for details, see the inset of Figure 2). This clearly indicates that sample 1s consists mostly of A2 aggregates. Since the concentration of trefoils and aggregates is very small (vide infra), intermolecular EET between aggregates and trefoils can be excluded. Finally, bleaching of type A1 aggregate is not clearly visible in broad nonresonant HB spectra because A1 aggregates are expected to be weakly red-shifted in comparison with ChlT1, and its hole could overlap with the antihole of ChlT1 and A2 aggregates. That is, the energy difference between the lowest energy state of ChlT1 and A1 must be relatively small. However, it cannot be excluded that the larger hole shift is caused in part by modified excitonic interaction in the A2-type aggregate.

The aggregate labeled A3 (peaking near 703 nm) most likely represents a dimer of ChlT1 trefoils. Dimers of Chl *a* with similar origin bands were reported in the literature and, depending on the nature of solvent composition, absorbed in the vicinity of 700−704 nm.[44,46,53,54] Different hole depths (see Figure 3B) near 710 nm in samples 1s and 2f clearly indicate different contributions from the A3 aggregates, where larger contributions are seen in the slowly cooled sample. We suggest the ∼710 nm state is the lowest excitonic state of A3 aggregates, with emission significantly red-shifted to ∼720 nm. Low-temperature emission from the A4 aggregate cannot be easily identified due to overlap with vibronic bands, although its absorption band near 740 nm has been clearly identified (see Figure 5A). Chl *a* aggregates with an origin band similar to the A4 aggregates were also reported in refs 45 and 53 The possible nature of A1−A4 trefoil aggregates is discussed in section 4.2. In summary, regarding fluorescence spectra shown in Figure 4, we hasten to add that major contributions in

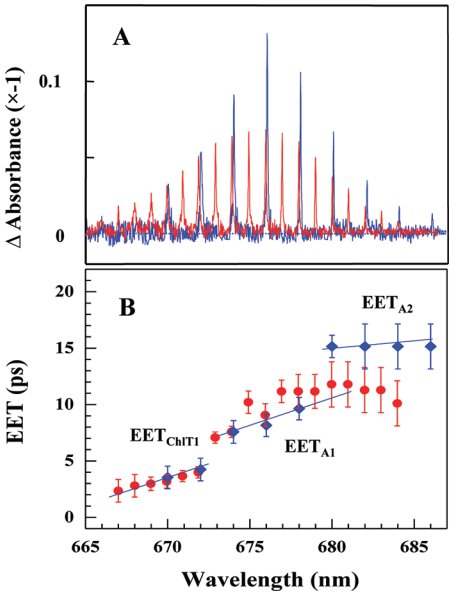

Figure 6. Frame A: Inverted zero-phonon-hole action spectra for samples 1s (blue spikes) and 2f (red spikes) at $T = 5$ K. Frame B: Plot of EET times as a function of burning wavelength for samples 1s (blue data points) and 2f (red data points). Solid lines in panel B are to guide the eye.

spectra a and b originate from ChlT1 and A2 aggregates, respectively. Finally, we consider the A3 aggregate emission band near 720 nm (see Table 1 for details) and note that a similar emission band was reported for Chl *a* dimers[45,54] that showed ∼725 nm fluorescence at 5 K

The shallowest hole in the fast-cooled sample (see curve 1 in Figure 2B) has the same position as that of the (0, 0)-emission band. This indicates, as already mentioned above, the shallowest hole is contributed to by slightly red-shifted A1 aggregates; however, they are not resolved in fluorescence spectra and exhibit relatively low fluorescence quantum efficiency when compared with trefoils (ChlT1). Thus, we conclude that the fluorescence spectrum observed for fast-cooled samples is mostly contributed to by monomer trefoils (ChlT1), whereas the slowly cooled samples show emission from the A2 aggregate. The latter is also consistent with ZPH action spectra shown in Figure 6A.

dx.doi.org/10.1021/jp2027252 |*J. Phys. Chem. B* 2011, 115, 10391–10399

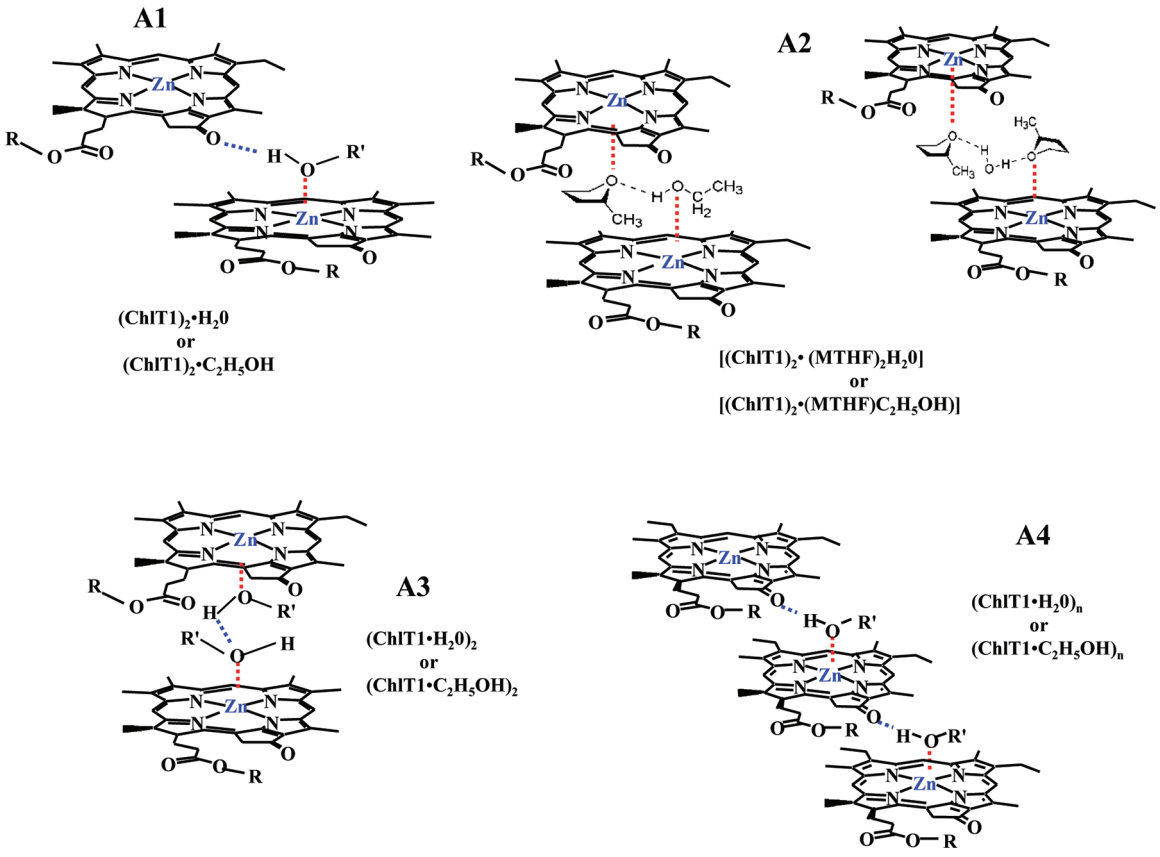

Figure 7. Possible nature of the A1−A4 aggregates. R′ could be either H or C_2H_5. R is the long hydrocarbon tail of a chlorophyll unit. For simplicity, only one subunit of each trefoil is shown to participate in aggregate formation. However, participation of multiple Zn−Chl units in aggregate formation is highly feasible.

4.2. Room Temperature Study and Nature of A1−A4 Aggregates. Taken as a whole, data presented in Figure 5A establish that aggregation increases with water concentration. The absorption spectrum without water (spectrum a) appears to be weakly aggregated with an absorption maximum near 670 nm. The latter band is red-shifted by ~5 nm in comparison with that reported in THF[23] at room temperature. This is caused by an increased polarity of ethanol in our matrix due to the solvatochromic shift. Comparison of spectra a−d reveals clearly that four types of aggregates (i.e., A1−A4) are continuously formed at the expense of the monomer trefoils. It is interesting to note the 740 nm band is already observed in spectra a and b. Due to the very large red shift of this absorption band, we assign such species to A4-type aggregates that correspond to oligomers with water or ethanol linkers, leading to $(ChlT1 \cdot H_2O)_n$ or $(ChlT1 \cdot C_2H_5OH)_n$ nanostructures, or both.

The broad feature around 700−705 nm also increases with water concentration; this type of aggregate (assigned to A3 type) could be due to strongly interacting ChlT1 in several different configurations; one of them (a symmetrical sandwich) is illustrated in Figure 7. Two possible linkers in our matrix may lead to the following types of A3 aggregates: $(ChlT1 \cdot H_2O)_2$ or $(ChlT1 \cdot C_2H_5OH)_2$. A3-type aggregates for Chl *a* molecules (with absorption near 700 nm) have also been observed and are well characterized in the literature.[45,46,48] Therefore, it is not surprising that such aggregates (with an origin band near 703 nm) are observed in our aggregated trefoil samples. Certainly, this type of association offers maximum stacking between chlorin macrocycles, so they are the most red-shifted dimers.

Regarding the composition of A2-type aggregates, on the basis of the position of the absorption origin band, we propose a structure similar to that observed for Chl *a* aggregates formed in aqueous THF solution.[49] That is, we assume that A2-type aggregate, again with two different linkers, $[(ChlT1)_2 \cdot (MTHF)_2 \cdot H_2O]$ or $[(ChlT1)_2 \cdot (MTHF)C_2H_5OH]$, can be formed by a direct link of the chlorin macrocycle centers, as shown in Figure 7. The latter would lead to diminished stacking (due to a larger distance between macrocycles) and a smaller red shift of the origin band than that observed in A3-type aggregates, in agreement with our experimental observations.

Finally, we suggest that $(ChlT1)_2 \cdot H_2O$ constitutes an A1-type aggregate in which the −C═O group of zinc chlorin of one ChlT1 subunit is H−bonded to water, and the water oxygen coordinates with the central zinc atom of the chlorin subunit belonging to next ChlT1 (see Figure 7). As a result, this type of aggregate does not have strong stacking interactions between the chlorin macrocycles, with a blue-shifted origin band in comparison with the A2-, A3-, and A4-type aggregates, in agreement with our assignment.

Since each ChlT1 molecule contains three identical Zn−Chls equally capable of forming aggregates, all of these subunits can be involved in aggregate formation, leading to various types of aggregate configurations. Because of this complex aggregation pattern, ChlT1 studied in this work represents excellent building blocks for construction of large, functional photosynthetic antenna systems.

A Gaussian fit to room temperature spectrum d of Figure 5 (not shown for brevity) also revealed five contributions: (i) ChlT1 with a band near 670 nm and (ii) four types of aggregates, A1, A2, A3, and A4, with origin bands near 673, 682, 701, and 740 nm, respectively, although at different ratios, proving that these aggregates are also formed at room temperature. Interestingly, similar band positions were also observed at room and low temperatures for various aggregates of Chl *a* molecules in different solvents.[44−54]

Additional support for aggregation of ChlT1 can be obtained from the resonance Raman (RR) spectrum shown in Figure 5B. As demonstrated above, most of the ChlT1 should be aggregated in our solvent mixture (MTHF, ethanol, and water 1:45:45 v/v), given our trefoil concentration. Regarding the RR spectrum, we are specifically interested in four features of the 1640−1700 cm^{-1} modes that describe the frequency of the −C═O stretching mode. On the basis of the literature data,[51] one could suggest the feature near 1700 cm^{-1} originates from a free −C═O group, whereas strongly downshifted modes (i.e. ∼1670, 1657, and 1648 cm^{-1}) originate from hydrogen-bonded −C═O groups. Both water and ethanol are capable of H-bonding with keto carbonyl groups. A keto carbonyl hydrogen bonded via water (−C═O···HOH) is expected to be the most downshifted, so we suggest that the 1648 cm^{-1} mode is an indicator of the $(ChlT1\cdot H_2O)_n$-type aggregate (i.e., A4). It was reported in ref 51 that $(Chl\cdot 2H_2O)_n$ aggregates possess the stretching frequency of keto carbonyl near 1645 cm^{-1}, in agreement with our assignment. The presence of 1657 and 1670 cm^{-1} bands in the Raman spectrum is also consistent with the formation of A4 and A1 aggregates with ethanol (−C═O···HOC_2H_5) and H_2O/ethanol linkers, respectively.

4.3. ZPH Action Spectra and EET Times. The presence of deeper zero-phonon holes (see blue spikes in Figure 6A) in the spectral range 675−685 nm in a slowly cooled sample (1s) is consistent with the relatively stronger absorption near 682.5 nm, as observed in Figure 2A. EET times for samples 1s and 2f vary from ∼2.5−11.0 ps (red data points in frame B of Figure 6) and 2.5−15.0 ps (blue data points), respectively. Interestingly, the EET time is slower at longer wavelengths, that is, where type A1 and A2 aggregates contribute. Resonant holes burned in the 667−686 nm range revealed that the EET time in the region where mostly ethynyl-linked chlorophyll trefoils (ChlT1) contribute is ultrafast (∼2.5 ps), at least at liquid helium temperatures, in agreement with femtosecond transient spectroscopy measurements obtained at room temperature, at which an EET time of 1.8 ps was observed.[23] A slowly cooled sample has more A2 aggregates where EET time is slower (i.e., about ∼15 ps).

In the region where there are several contributing assemblies, that is, in the 670−680 nm spectral range, intermediate EET time values are observed, depending on the aggregates' composition. Note that the EET time in A1 and A2 aggregates decreases only by a factor of ∼5−7 with respect to that observed for monomer trefoils. Apparently, donor−acceptor distance and relative orientation of their transition dipoles are responsible for the observed difference in EET between ChlT1 and type A1 and A2 aggregates. This most likely is the reason why observed EET times are strongly dependent on the burning wavelength. These results are consistent with data presented in Figures 2, 3, and 4.

It is of interest to note that the ultrafast EET times in ChlT1, A1, and A2 aggregates are comparable to that observed in various natural photosynthetic antennae.[33−36,42,43,55−62] We hasten to add that an ultrafast EET time in trefoils can have, as discussed in ref 23, both through-bond[63] and through-space[64] contributions. Note that through-space (Förster) EET originates from the dipole−dipole approximation of the Coulombic interactions. If the donor−acceptor distance is relatively short and the coupling between chromophores is weak, the excitation energy can hop from the donor to the acceptor site through space. This type of EET can be described by the Förster theory.[64] Through-bond EET (Dexter type[63]) requires sufficient overlap of the electronic wave functions and is observed at relatively shorter distances than Förster EET. In the case of ChlT1 monomer, the interchromophore distance is ∼15 Å, so one expects to have weak coupling matrix elements and, as a result, relatively slow Förster EET. However the chromophores in ChlT1 are coupled via a rigid linker, allowing a significant contribution from Dexter EET.

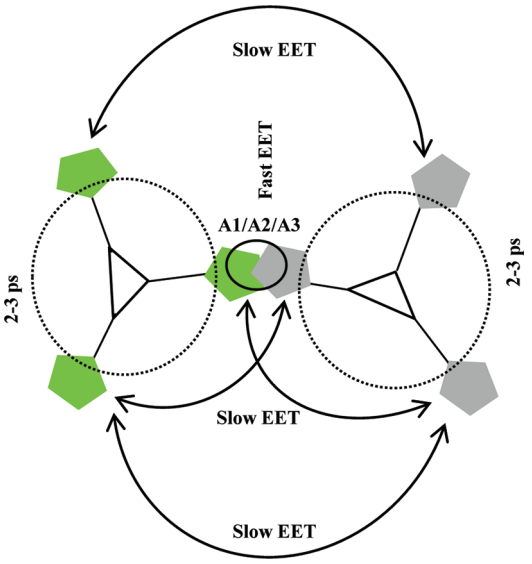

Figure 8. Possible model of EET in ChlT1 aggregates; Zn−Chls and rigid linkers are represented by pentagons and triangles, respectively. Zn−Chls belonging to the same trefoil are shown in the same color.

In general, EET in ChlT1 can be understood as exciton hopping from one to another subunit. However, in ChlT1 aggregates, several possible EET pathways can exist, as summarized in Figure 7. A simple model shown in Figure 8 further illustrates possible pathways of EET in A1-, A2-, or A3-type aggregates. In this figure, Zn−Chls belonging to the same trefoils are shown in the same color. The EET time between Zn−Chls belonging to the same trefoil is indicated by dotted circles. The EET time can be fast because chromophores are coupled via a rigid linker and due to a relatively short (∼15 Å) distance between the donor and acceptor. Most likely, this EET time slows down when one (or all) of the subunits is (are) engaged in formation of A1/A2/A3 aggregates and could be slower in comparison to EET time observed in a monomer trefoil. EET between zinc subunits belonging to two different trefoils involved in aggregate formation (as indicated by a small solid circle) can still be fast because of a relatively short donor−acceptor distance. That is, as reported in ref 48 for Chl *a* dimers, analogous to our A3-type aggregate, the center-to-center Chl distance is only ∼6.5 Å. In the case of A1 and A2 aggregates this distance can be larger than 6.5 Å, but still short enough to allow a fast through-space EET.

Long-range (slow) EET pathways (through space) are also possible, as indicated by the double-sided solid arrows in Figure 8. These pathways seem feasible, at least in terms of distance because

the donor−acceptor distance between Zn−Chls can be larger than 15 Å for noncovalently linked moieties. The time scale of the above-mentioned EET pathways could be very different if two or three Zn−Chl subunits are involved in aggregate formation. In addition, the presence of different facial isomers and, hence, different EET pathways cannot be excluded. In fact, the range of EET times (see Figure 6B) is consistent with several contributions. We note that very fast and very slow EET times reported in ref 65 for ChlT2 aggregates (using time-domain spectroscopy) are also consistent with the large range of the EET times observed in this work.

5. CONCLUSIONS

It has been shown that the ChlT1 trefoil (consisting of three identical Zn−Chls) is capable of aggregate formation. Four types of aggregates (A1−A4) were identified in matrixes with an increasing concentration of water. Aggregation is consistent with Raman spectra in which multiple, significantly downshifted −C═O stretching bands were observed. It was shown that the degree of aggregation strongly depends on the rate of cooling. We conclude that fast-cooled samples contain a population of solvated trefoils (ChlT1) and A1/A2 aggregates, whereas slowly cooled samples are dominated by A2 aggregates with a smaller contribution from solvated ChlT1 and A1 aggregates. EET times obtained from ZPHs revealed three major groups of EET times consistent with the presence of a mixture of ChlT1, A1, and A2 aggregates. The latter is consistent with absorption, emission, and nonresonant HB spectra. The EET time in ChlT1 is ∼2.5 ps and slows down by a factor of 5−7 in A1- and A2-type aggregates. These fast EET times observed in A1 and A2 aggregates are of interest because they are comparable to those observed in various natural photosynthetic antenna complexes.[33−36,43] In this regard, we predict the trefoil studied in this work, in suitable solvents, will form three-dimensional building blocks capable of very efficient EET (research in progress). It is anticipated that such building blocks, mimicking natural photosynthetic antenna systems, could be used in future photovoltaic devices.

AUTHOR INFORMATION

Corresponding Author

*E-mail: ryszard@ksu.edu.

Present Addresses

§Los Alamos National Laboratory, Los Alamos, NM 87544

ACKNOWLEDGMENT

This work was supported by the DOE EPSCoR (DE-FG02-08ER46504) Grant (R.J.) and in part by the State of Kansas through the Kansas Technology Enterprise Corporation. Work at Northwestern University (M.R.W.) was supported by the Division of Chemical Sciences, Office of Basic Energy Science, DOE under Grant no. DE-FG02-99ER14999. We also acknowledge Dr. Bret Flanders (Department of Physics, KSU) for the measurement of the resonant Raman spectra of a trefoil samples.

REFERENCES

(1) Witt, H. T.; Müller, A.; Rumberg, B. *Nature* **1963**, *197*, 987–991.
(2) Barber, J. *Q. Rev. Biophys.* **2003**, *36*, 71–89.
(3) Fromme, P. *Photosynthetic Protein Complexes: A Structural Approach*, Wiley-VCH VerlagGmbH&Co. KGaA: Berlin, Germany, 2008; pp 1−100.
(4) Blankenship, R. E. *Molecular Mechanisms of Photosynthesis*; Blackwell Science Ltd.: London, 2008; pp 42−95.
(5) D'Souza, F.; Smith, P. M.; Zandler, M. E.; McCarty, A. L.; Itou, M.; Araki, Y.; Ito, O. *J. Am. Chem. Soc.* **2004**, *126*, 7898–7907.
(6) Lee, A. J.; Ensign, A. A.; Krauss, T. D.; Bren, K. L. *J. Am. Chem. Soc.* **2010**, *132*, 1752–1753.
(7) Hindin, E.; Kirmaier, C.; Diers, J. R.; Tomizaki, K.; Taniguchi, M.; Lindsey, J. S.; Bocian, D. F.; Holten, D. *J. Phys. Chem. B* **2004**, *108*, 8190–8200.
(8) Yatskou, M. M.; Koehorst, R. B. M.; van Hoek, A.; Donker, H.; Schaafsma, T. J.; Gobets, B.; van Stokkum, I.; van Grondelle, R. *J. Phys. Chem. A* **2001**, *105*, 11432–11440.
(9) Nakamura, Y.; Hwang, I.-W.; Aratani, N.; Ahn, T. K.; Ko, D. M.; Takagi, A.; Matsumoto, T.; Kim, D.; Osuka, A. *J. Am. Chem. Soc.* **2005**, *127*, 236–246.
(10) Luo, C.; Guldi, D. M.; Imahori, H.; Tamaki, K.; Sakata, Y. *J. Am. Chem. Soc.* **2000**, *122*, 6553–6551.
(11) Kobuke, Y. *Eur. J. Inorg. Chem.* **2006**, 2333–2351.
(12) Imahori, H.; Fukuzumi, S. *Adv. Funct. Mater.* **2004**, *14*, 525–536.
(13) Noy, D.; Moser, C. C.; Dutton, P. L. *Biochim. Biophys. Acta* **2006**, *1757*, 90–105.
(14) Kamat, P. V. *J. Phys. Chem. C* **2007**, *111*, 2834–2860.
(15) Barbour, L. W.; Hegadorn, M.; Asbury, J. B. *J. Am. Chem. Soc.* **2007**, *129*, 15884–15894.
(16) Forrest, S. R. *MRS Bull.* **2005**, *30*, 28–32.
(17) Gledhill, S. E.; Scott, B.; Gregg, B. A. *J. Mater. Res.* **2005**, *20*, 3167–3179.
(18) Huijser, A.; Savenije, T. J.; Kotlewski, A.; Picken, S. J.; Siebbeles, L. D. A. *Adv. Mater.* **2006**, *18*, 2234–2239.
(19) Samuel, A. P. S.; Co, D. T.; Stern, C. L.; Wasielewski, M. R. *J. Am. Chem. Soc.* **2010**, *132*, 8813–8815.
(20) Wasielewski, M. R. *J. Org. Chem.* **2006**, *71*, 5051–5066.
(21) Garg, V.; Kodis, G.; Chachisvilis, M.; Hambourger, M.; Moore, A. L; Moore, T. A.; Gust, D. *J. Am. Chem. Soc.* **2011**, *133*, 2944–2954.
(22) Terazono, Y.; Kodis, G.; Bhushan, K.; Zaks, J.; Madden, C.; Moore, A. L; Moore, T. A.; Fleming, G. R.; Gust, D. *J. Am. Chem. Soc.* **2011**, *133*, 2916–2922.
(23) Kelley, R. F.; Tauber, M. J.; Wasielewski, M. R. *Angew. Chem., Int. Ed.* **2006**, *45*, 7979–7982.
(24) Fenna, R. E.; Matthews, B. W. *Nature* **1975**, *258*, 573–577.
(25) Hu, X.; Ritz, T.; Damjanović, A.; Autenrieth, F.; Schulten, K. *Q. Rev. Biophys.* **2002**, *35*, 1–62.
(26) Jordan, P.; Fromme, P.; Witt, H. T.; Klukus, O.; Saenger, W.; Krauβ, N. *Nature* **2001**, *411*, 901–917.
(27) Liu, Z.; Yan, H.; Wang, K.; Kuang, T.; Zhang, J.; Gui, L.; An, X.; Chang, W. *Nature* **2004**, *428*, 287–292.
(28) Guskov, A.; Kern, J.; Gabdulkhakov, A.; Broser, M.; Zouni, A.; Saenger, W. *Nat. Struct. Mol. Biol.* **2009**, *16*, 334–342.
(29) Loll, B.; Kern, J.; Saenger, W.; Zouni, A.; Biesiadka, J. *Nature* **2005**, *438*, 1040–1044.
(30) Brixner, T.; Stenger, J.; Vaswani, H. M.; Cho, M.; Blankenship, R. E.; Fleming, G. R. *Nature* **2005**, *434*, 625–628.
(31) Groot, M.; Frese, R. N.; de Weerd, F. L.; Bromek, K.; Pettersson, A.; Peterman, E. J. G.; van Stokkum, I. H. M.; van Grondelle, R.; Dekker, J. P. *Biophys. J.* **1999**, *77*, 3328–3340.
(32) Prokhorenko, V. I.; Holzwarth, A. R. *J. Phys. Chem. B* **2000**, *104*, 11563–11577.
(33) Renger, T.; Schlodder, E. *ChemPhysChem* **2010**, *11*, 1141–1153.
(34) Hughes, J. L.; Prince, B. J.; Krausz, E.; Smith, P. J.; Pace, R. J.; Riesen, H. *J. Phys. Chem. B* **2004**, *108*, 10428–10439.
(35) Dang, N. C.; Zazubovich, V.; Reppert, M.; Neupane, B.; Picorel, R.; Seibert, M.; Jankowiak, R. *J. Phys. Chem. B* **2008**, *112*, 9921–9933.
(36) Neupane, B.; Dang, N. C.; Acharya, K.; Reppert, M.; Zazubovich, V.; Picorel, R.; Seibert, M.; Jankowiak, R. *J. Am. Chem. Soc.* **2010**, *132*, 4214–4229.

(37) Rätsep, M.; Pieper, J.; Irrgang, K. D.; Freiberg, A. *J. Phys. Chem. B* **2008**, *112*, 110–118.
(38) Berlin, Y.; Burin, A.; Friedrich, J.; Köhler, J. *Phys. L. Rev.* **2007**, *4*, 64–89.
(39) Lee, J.-E.; Yang, J.; Gunderson, V. L.; Wasielewski, M. R.; Kim, D. *Phys. Chem. Lett.* **2010**, *1*, 284–289.
(40) Moerner, W. E. *Topics in current physics, Persistent spectral hole burning: Science and applications*; Springer-Verlag: New York, 1987; pp 1−19.
(41) Jankowiak, R.; Hayes, J. M.; Small, G. J. *Chem. Rev* **1993**, *93*, 1471–1502.
(42) Purchase, R.; Völker, S. *Photosynth. Res.* **2009**, *101*, 245–266.
(43) Jankowiak, R.; Reppert, M.; Zazubovich, V.; Pieper, J.; Reinot, T. *Chem. Rev.* **2011**, *111*, 4546–4598.
(44) Cotton, T. M; Loach, P. A.; Katz, J. J; Ballschmiter, K. *Photochem. Photobiol.* **1978**, *27*, 735–749.
(45) Fong, F. K.; Koester, V. J. *Biochim. Biophys. Acta* **1976**, *423*, 52–64.
(46) Fong, F. K.; Koester, V. J. *J. Am. Chem. Soc.* **1975**, *97*, 6888–6890.
(47) Fong, F. K.; Wassam, W. A. *J. Am. Chem. Soc.* **1977**, *99*, 2375–2376.
(48) Koester, V. J.; Fong, F. K. *J. Phys. Chem.* **1976**, *80*, 2310–2312.
(49) Uehara, K.; Hioki, Y.; Mimuro, M. *Photochem. Photobiol.* **1993**, *58*, 127–132.
(50) Brody, S. S.; Broyde, S. B. *Biophys. J.* **1968**, *8*, 1511–1533.
(51) Koyama, Y.; Umemoto, Y.; Akamatsu, A. *J. Mol. Struct.* **1986**, *146*, 273–287.
(52) Agostiano, A.; Cosma, P.; Trotta, M.; Monsù-Scolaro, L.; Micali, N. *J. Phys. Chem. B* **2002**, *106*, 12820–12829.
(53) Koester, V. J.; Polles, J. S.; Koren, J. G.; Galloway, L.; Andrews, R. A.; Fong., F. K. *J. Lumin.* **1976**, *12/13*, 781–786.
(54) Kooyman, R. P. H.; Schaafsma, T. J.; Kleibeuker, J. F. *J. Photochem. Photobiol.* **1977**, *26*, 235–240.
(55) Melkozernov, A. N.; Bibby, T. S.; Lin, S.; Barber, J.; Blankenship, R. E. *Biochemistry* **2003**, *42*, 3893–3903.
(56) Riley, K. J.; Zazubovich, V.; Jankowiak, R. *J. Phys. Chem. B* **2006**, *110*, 22436–22446.
(57) Damjanović, A.; Vaswani, H. M.; Fromme, P.; Fleming, G. R. *J. Phys. Chem. B* **2002**, *106*, 10251–10262.
(58) Thangaraj, B.; Jolley, C. C.; Sarrou, I.; Baltema, J. B.; Greyslak, J.; Whitelegge, J. J.; Lin, S.; Kouřill, R.; Subramanyam, R.; Boekema, E. J.; Fromme, P. *Biophys. J.* **2010**, *99*, 1–9.
(59) Feng, X.; Neupane, B.; Acharya, K.; Zazubovich, V.; Picorel, R.; Seibert, M.; Jankowiak, R. *J. Phys. Chem. B* **2011**submitted.
(60) Pawlowicz, N. P.; Groot, M.-L.; van Stokkum, I. H. M.; Breton, J.; van Grondelle, R. *Biophys. J.* **2007**, *93*, 2732–2742.
(61) Franken, E. M.; Neerken, S.; Louwe, R. J. W.; Amesz, J.; Aartsma, T. J. *Biochemistry* **1998**, *37*, 5046–5051.
(62) Milder, M. T. W.; Bruggemann, B.; van Grondelle, R.; Herek, J. L. *Photosynth. Res.* **2010**, *104*, 257–274.
(63) Dexter, D. *J. Chem. Phys.* **1953**, *21*, 836–850.
(64) Förster, T. *Ann. Phys. (Leipzig)* **1984**, *2*, 55–75.
(65) Gunderson, V. L.; Conron, S. M. M.; Wasielewski, M. R. *Chem. Commun.* **2010**, *46*, 401–403.